size 89 μm as a counterface material. They have reported that the Ni addition not only enhances wear resistance but also increases the friction coefficient during sliding wear test. Sudhakar *et al.*[6] have studied the wear behavior of Fe-0.2%Ni-0.47%C and Fe-0.2%Ni-0.2%C P/M alloy materials at various heat treatments and have used alloy steel plate of hardness 62 HRC as a counterface body. They have observed that the delamination wear is predominant in the as sintered specimen and oxidative wear is dominant in the hardened and tempered specimens. Wang *et al.*[7] have studied the tribological behavior of copper added titanium alloy with ZrO_2 balls of 5 mm diameter using the universal multifunctional tester. They observed that the Cu addition invariably enhances the wear resistance of the alloy steel and both adhesive and abrasive wear are observed as wear mechanism in the material. Qiu *et al.* [8] have conducted dry sliding wear tests on Ti-47Al-2Cr-2Nb-0.2W (at. %) alloy at four different environments using yttria-stabilished zirconia as a counter body for the tribological study. They have found that the oxygen environment exhibits a lower wear rate and hydrogen environment has little effect on wear rate. Wang *et al.*[9] have studied the influence of various heat treatments on wear behavior of Fe-1%C-3.5%Mo alloy steel and have used 100Cr6 with a hardness of 62-63 HRC as a counter disc. They have reported that the quenched and tempered specimen is subjected to higher wear coefficient compared to the as sintered specimen. They have also reported that the alloy steel exhibits a low and stable wear rate. Tekeli *et al.*[10] have analyzed the tribological behavior of Fe-C-Ni steel under various heat treatments. They were used alloy steel plate of hardness 55 HRC as the counterface material. They have found that the inter-critically annealed specimen exhibits higher hardness and strength than the other heat treated specimens and also reported that the same specimen exhibits a lower wear rate. Anton *et al.*[11] have investigated the tribological behavior of sintered steels with a high content of manganese-nickel and the linear dry sliding test was conducted using a spherical pin of martensitic steel of hardness 49 HRC. They have found that the addition of C and Mn increases the wear resistance of the alloy. Vijay and Kandavel[12] have studied the application of Artificial Neural Network (ANN) on wear properties of sinter-forged Fe-C-Mo low alloy steel against EN 31 alloy steel. The wear resistance of low alloy steel is found to be greater due to the formation of the hard phases, Mo particulates and its carbides in the microstructure. Ceschini *et al.* [13] have investigated the wear behavior of Fe-C-Mo and Fe-C-Cr P/M alloy steels at various sintered temperatures and have used martensitic steel ball of hardness 900 HV for the wear test. They have reported that Mo alloyed steel has a higher hardness than the other alloy steel and mild oxidative wear is found as common wear mechanism at lower load (the load lesser than the average load) and delamination wear is common at the higher load conditions for the alloy steels. Kandavel *et al.* [14] have studied the plastic deformation and densification of Fe-C-Cu-Mo-Ti sintered alloy steels. They have stated that the addition of alloying elements invariably enhances the hardness of the alloy steel, which in turn may enhance the wear resistance of the alloy steels. Rajan *et al.*[15] have investigated the tribological behavior of Cu-10%W composite and they have used EN 31 steel of hardness 64 HRC as a counter body in the test. They have reported that increasing the sliding distance increases the volume loss of wear and decreases the friction coefficient. Chotibhawaris and Laungwaranant[16] have studied the wear behavior of P/M tin-bronze material against 304 stainless steel and have found that the wear rate is decreased due to the transfer layer formed by adhesion and have also found that abrasive and fatigue wear mechanisms are predominant in the material. Luangvaranunt and Pripanapong[17] have investigated the wear properties of Ti-Cu alloys under precipitation hardening and ageing heat treatment and have used 304 stainless steel as a counterface material. They have observed that though the hardness of alloy is enhanced, the wear resistance property is deteriorated due to the formation of a lamellar microstructure. Bidulský *et al.*[18] have studied the wear properties of Cr-C alloy coated with TiCN and WC-Co pin was used as a counterface material. They have found that the wear resistance of coated alloy material is enhanced due to the formation bainitic microstructure. They have also found that the delamination and oxidation wear are the predominant wear mechanisms in the material. Vettivel *et al.*[19] have investigated the wear properties of Cu-W composites at various densities and sintering temperatures against EN 31 disc as a counterface material. They have reported that the severe metallic wear has occurred for the specimen sintered at the higher temperature and at the higher sliding distance. They have applied Artificial Neural Network and developed a model for predicting the response parameters for non-conducted working parameters of tests.

In the present work, the influence of Ti and W on dry sliding wear characteristics of the P/M plain carbon steel has been investigated. The mathematical correlations to find the wear loss and coefficient of friction for the alloy steels have been generated by the DE software. The artificial neural network has been applied to predict the wear behavior of the P/M alloy steels. The response values of the experiments have been compared with the predicted values of mathematical correlations and ANN to find the suitability for wear behavior of the alloy steels.

2 Materials and Methods

High quality powders of elements such as iron (Fe), graphite (C), tungsten (W) and titanium (Ti) were weighed accurately and mixed homogeneously using a pot mill in order to obtain the alloy powders of Fe-1%C, Fe-1%C-1%Ti, Fe-1%C-1%W, and Fe-1%C-1%Ti-1%W. The homogeneously mixed alloy compositions were then compacted into cylindrical billets (Ø25×33mm^2) using a cylindrical die-punch set of the same size in a 100T (1000kN) capacity hydraulic press. Graphite and oil were used as a lubricant during compaction. The uni-axial load of 18T (180kN) was gradually applied to obtain 85% theoretical density of green compacts of alloy steel preforms. The indigenously made ceramic coating was applied over the exposed surface of the green compact specimens to prevent the surface oxidation during the sintering process. Sintering was carried out in a 3.5 kW electric muffle furnace at a temperature of 1100 ±10 °C for a period of 30 minutes and the samples were kept in the furnace until they were cooled. The sintered specimens were once again heated to a temperature of 1000 °C and hot upsetting was carried out on the heated specimens to convert it into a square rod of size 10X75 mm^2. Hot upsetting is one of the secondary operations performed particularly on the P/M material to enhance their density. The machining operation was carried out on the square specimens to get standard wear test specimens of size Ø6×50 mm^2. The hardness of the as sintered and test specimens was found out using a microhardness tester (Vickers hardness tester). The contact surface of the pin was polished using various grades of emery sheets to conduct dry sliding wear test. Pin-on-disc tribometer was used to conduct the experiment. EN 31 hardened steel disc (53.5 HRC) was used as a counter-face material for all the wear tests. The wear test was conducted by keeping the pin at a track radius of 17mm and maintained constant for the entire wear tests. The wear experiment was carried out as per the standard ASTM G99-05. The D-optimal design on response surface methodology (RSM) by Design Expert (DE) software was used to plan the experimental test and the tests were carried out based on the test plan provided by the DE software. In the present work, the load and speed are considered as input parameters and mass loss and friction coefficient are considered as output parameters. The load was set at a range of 15-50 N and speed was set at a range of 300-1200 rpm and keeping the time (30 min) constant for tests. The wear loss is calculated by measuring the mass of pin before and after the tests using a Shimadzu digital balance (Made in Japan). The friction coefficient was obtained from the computer system interface with the tribometer. The microstructure images of the P/M alloy steels and wear pattern of the test specimens were captured by KYOWA, ME-LUX2, microscope fitted with CCD camera. SEM images of maximum worn out specimens of alloy steels were captured by using a Field Emission Scanning Electron Microscope (JEOL - TSM-6701F). The optical wear images and microstructure of the alloy steels were correlated with the wear behavior of the P/M alloy steels. X-ray diffraction spectroscopy has been carried on the wear debris of the alloy steels in order to find the microelements present in the wear removed particles. Levenberg-Marquardt backpropagation algorithm of artificial neural network (ANN) software was applied to predict the wear characteristics of the alloy steels at any input parameters and also the ANN results are validated with the experimental findings.

2.1 Levenberg-Marquardt Back Propagation Algorithm

Levenberg-Marquardt backpropagation algorithm is the fastest backpropagation algorithm ever. These networks behave based on the desirability of the responses. The network divides the sample based on the percentage, likely 70% of data for training, which is utilized by the network and manipulates itself based on the faults, 15% of data for the purpose of validation and performance characteristics generalization and 15% of data for testing. The experimental results of the wear tests were used for providing input and response parameters for the ANN network. Two sorts of layers namely hidden and output layers are used. The input consists of two neurons, namely load (N) and speed (rpm). The output consists of two neurons such as mass loss (g) and coefficient of friction (μ). The hidden layers can

be adjusted so that minimal fault is observed in the output. The neurons are the functionary nodes which are found as an intermediating factor and interrelating modules. The neuron works based on the present input, the weighted function and the bias. These values are stored in the ANN. The training of neural network terminates on the condition when performance has reached the target, even when the maximum number of reputations is reached. The network structure of the ANN is clearly illustrated in Fig. 1.

The artificial neural network is applied in the present work to validate the experimental results and to predict the wear behavior of the P/M alloy steels at any given load and speed within the working ranges. In the present work, the wear properties are discussed based on the mass loss and the frictional force exerted during the wear test. The normalized data were fed into the ANN toolbox. The hidden layer used a TANSIG transfer function and a number of neurons were 15 and the output layers neuron was set as 2. The network system was trained using back propagation algorithm.

3 Results and Discussion

3.1 Variation of Hardness and Density of P/M Alloy Steels

Unlike solid metals, the densities as well as hardness of powder metallurgy (P/M) metals are increasing during plastic deformation. This unique feature of P/M materials has widened their applications in all industrial areas. Moreover, the mechanical properties are also improved after simultaneous plastic deformation and densification processes. The enhancement of hardness and density of the alloy steels after hot upsetting are provided in Table 1. It is observed from the table that there is a significant hardness improvement for the hot upset specimens compared to the as sintered preforms of the alloy steels. Similarly, due to plastic deformation, the density of alloy steels is also enhanced. For sintered preforms, the presence of pores is higher and inevitable. The pores are closed and coalesced when the preforms are subjected to hot upset. The pores closure in the preforms has led to enhancement of density. It is noticed from the table that the addition of alloying elements plays a vital role in enhancing the hardness of the alloy steels apart from densification and deformation processes. Tungsten alloyed steel has higher hardness compared to the titanium alloyed steel. Addition of tungsten and titanium invariably increases the hardness of the alloy steels. In nature, the alloying elements Ti and W are found to form carbide phases when chemically react with carbon.[15] This could be the reason for the highest hardness observed in the case of Fe-1%C-1%Ti-1%W P/M alloy steel.

3.2 Wear Rate Behavior of P/M Alloy Steels

The wear rate is one of the important response factors for wear studies. In machinery, each component has a relative motion to another and during a long period the wear loss due to friction with matting parts affect the normal functioning of the

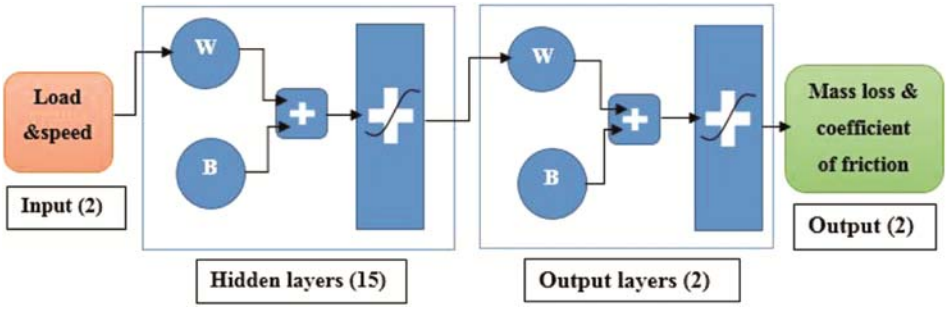

Fig. 1 — Artificial neural network (ANN) structure.

Table 1 — Microhardness and density of the P/M alloy steels.

Alloy compositions	Theoretical density (g/cc)	As sintered		Hot upset	
		Microhardness (HV)	%theoretical density	Microhardness (HV)	%theoretical density
Fe-1%C	7.67	167.5	86.44	247.5	98.95
Fe-1%C-1%Ti	7.62	204.5	85.43	302.5	99.40
Fe-1%C-1%W	7.72	263.5	84.44	327.5	99.22
Fe-1%C-1%Ti-1%W	7.66	292.5	84.72	360	99.66

component. It is essential that the study on wear rate behavior for any material is warranted. The wear characteristics of P/M material is a complex phenomenon due to the presence of pores at the contact surfaces. Table 2 provides the experimental results of P/M alloy steels. The wear rate characteristics of the alloy steels are illustrated in Figs 2(a)-(d). The general trend of wear rate behavior of the alloy steels is

Table 2 — Experimental results of the P/M alloy steels.

			Alloys compositions							
			Fe-1%C		Fe-1%C-1%Ti		Fe-1%C-1%W		Fe-1%C-1%Ti-1%W	
Runs	Load (N)	Speed (rpm)	Wear rate x 10^{-3} (g/N-h)	Coefficient of friction	Wear rate x 10^{-3} (g/N-h)	Coefficient of friction	Wear rate x 10^{-3} (g/N-h)	Coefficient of friction	Wear rate x 10^{-3} (g/N-h)	Coefficient of friction
1	15	300	0.2267	0.6186	0.0533	0.6331	0.0533	0.6652	0.0267	0.6544
2	26.67	300	0.225	0.5316	0.0975	0.5893	0.0825	0.4940	0.0375	0.6359
3	50	300	0.332	0.4747	0.116	0.4389	0.076	0.3767	0.052	0.3813
4	50	600	0.368	0.4989	0.132	0.4634	0.084	0.3483	0.064	0.3766
5	32.5	750	0.4615	0.5258	0.1538	0.5603	0.08	0.4493	0.0492	0.4895
6	15	900	0.92	0.5973	0.2533	0.6236	0.16	0.4888	0.0667	0.5944
7	15	1200	1.04	0.6004	0.32	0.6193	0.2267	0.3649	0.1333	0.3849
8	26.67	1200	0.6674	0.6281	0.2325	0.6530	0.1575	0.3603	0.105	0.3668
9	50	1200	0.416	0.4653	0.144	0.3513	0.096	0.3480	0.076	0.3659

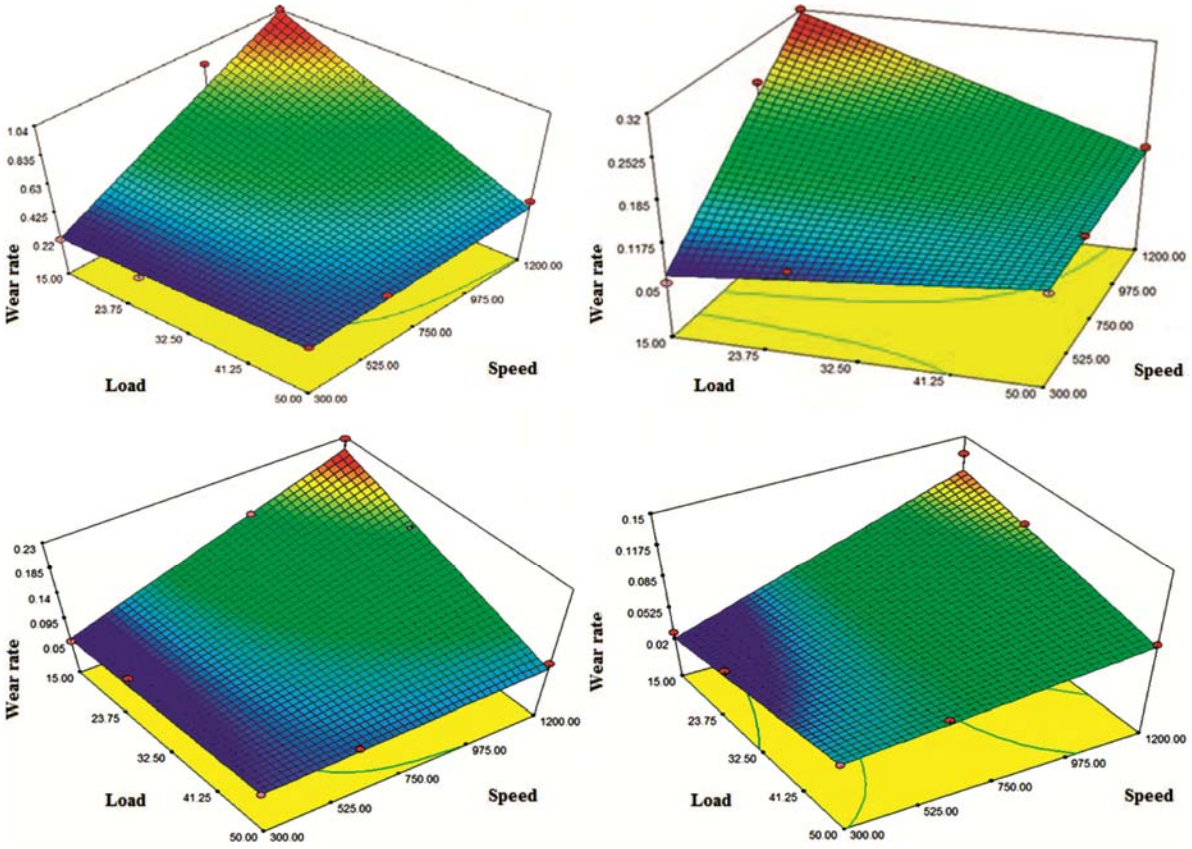

Fig. 2 — 3D surface contour plot of wear rate characteristics of the P/M alloy steels (a) Fe-1%C, (b) Fe-1%C-1%Ti, (c) Fe-1%C-1%W and (d) Fe-1%C-1%W-1%Ti.

observed to be similar. Increasing the input parameters such as either load or speed increases the wear rate of the material. However, the maximum and minimum wear rates exhibited by the alloy steel compositions are varied and determined by the alloying elements compounded in the alloy steels. The wear rate characteristic of the plain carbon steel is shown in Fig. 2(a). The minimum wear rate is observed at the lowest load and speed conditions. The maximum wear rate ($1.04x10^{-3}$g/N-h) is exhibited at the 15 N load and 1200 rpm speed. Increasing any single working parameter such as load or speed is observed to increase the wear rate, not to a significant level. The same kind of trend is observed irrespective of the alloy steels. At the higher load and higher speed, the increasing of wear rate is not to appreciable level. On the other hand, at the lowest load (15 N) and the highest speed (1200 rpm), the wear rate is found to have maximum. At the lower axial load/force, the intimate contact between mating surfaces is minimum, which leads to continuous removal of material from the specimen surface. In contrast, at the higher axial load/force condition, the contact between the surfaces is intimate and there is a possibility of trapping of wear debris in the voids region, which leads to reducing the wear rate of the alloy steel. The same kind of wear rate behavior phenomenon is observed for all the alloy steels. As the wear rate is continuously increasing with respect to the working parameters, the wear mechanism could be the delamination for all the alloy steels. The 3D contour surface for the wear rate behavior of the Ti alloyed plain carbon steel is shown in Fig. 2(b). The maximum wear rate ($0.32x10^{-3}$g/N-h) is found at the 15 N load and 1200 rpm speed. 69% wear rate reduction is found compared to the plain carbon steel. Addition of Ti element to the plain carbon steel plays a significant role in increasing the wear resistance of the alloy steel. The wear rate behavior of W added plain carbon steel is shown in Fig. 2 (c). Though the wear rate trend is similar to the plain carbon and Ti alloyed steels, the maximum wear rate ($0.2267x10^{-3}$g/N-h) is observed at the least and the highest load and speed respectively. It is found from the values that the wear rate is decreased by 78% and 29% when compared to the plain carbon steel and Ti alloyed steel respectively. It is understood from the observation that the addition of tungsten to the plain carbon steel significantly enhances the wear resistance of the alloy steel. The wear rate behavior of Fe-1%C-1%Ti-1%W P/M alloy steel is shown in Fig. 2(d). It is observed from the plot that the wear rate is reduced to the greater extent compared to the alloy steels. The combined positive effects of both the alloy elements (Ti and W) enhance the wear resistance of the alloy steel to the maximum possible level. The maximum wear rate observed for the alloy steel is $0.1333x10^{-3}$g/N-h. It is found from the wear rate values that the wear rate is reduced by 87%, 58% and 41% when compared to the plain carbon steel, Ti alloyed steel and W alloyed steel respectively. The alloy steel containing Ti and W has better wear resistance property and it could be a better candidate for a cutting tool.

3.3 Coefficient of Friction of P/M Alloy Steels

Figures 3(a & b) illustrate the characteristics of the coefficient of friction of the P/M alloy steels. There is an unique property observed from the plots that the frictional force exerted by the alloy steels during wear test is found to be lower at the highest load and speed conditions. Figure 3(a) shows the frictional characteristics of the plain carbon steel. Initially, the friction between the contact surfaces is more, and it is declining with the increase in load and mounting up further with an increase in speed. It is observed from the plot that the minimum frictional coefficient is exhibited at the highest load irrespective of the speed. The variation of frictional coefficient along the various speeds is observed to be minimal. The highest frictional force is exerted at the highest speed condition. Sliding speed is playing an important role in frictional force rather than the axial load. The frictional coefficient is continuously varying in the plain carbon steel due to delamination wear character of the alloy steel. The coefficient of friction characteristic of Ti added plain carbon steel is shown in Fig. 3(b). Though the trend seems like a base metal, the friction coefficient exhibited by the alloy steel is higher. It is observed from the plots that the frictional coefficient is higher for a particular value of the load and then descending to the minimum irrespective of speed. The higher frictional value is due to the presence of carbides in the alloy steel. At the higher load, the contact surface becomes polished, which in turn reduces the friction during wear test.

The frictional characteristics of W added plain carbon steel is shown in Fig. 3(c). The peculiar coefficient of friction property is observed in the alloy steel. The coefficient of friction exerted between the mating surfaces is observed to be decreased with an

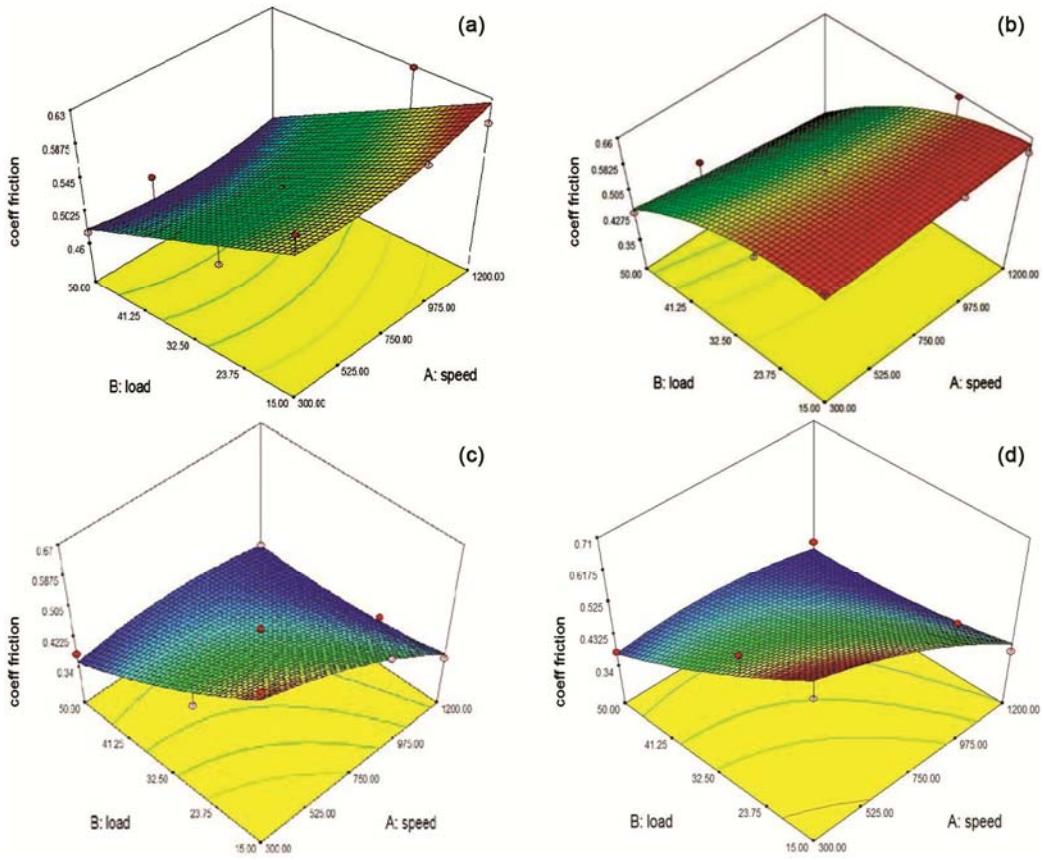

Fig. 3 — 3D surface contour plot of coefficient of friction characteristics of the P/M alloy steels (a) Fe-1%C, (b) Fe-1%C-1%Ti, (c) Fe-1%C-1%W and (d) Fe-1%C-1%W-1%Ti.

increase in load and speed. The strong hard phases formed in the alloy steel could be the reason for the reduction of frictional force during the wear test. The hard phase becomes smoother during the test and contributes to the lesser frictional force. The trend of the coefficient of friction with respect to load and speed of Ti and W added plain carbon steel is illustrated in the Fig. 3(d). Though the trend is similar to W added alloy steel, the values of coefficient of friction are observed to be little higher than ones found for the W alloyed steel. The higher coefficient of friction values is due to the abrasive action of hard particles due to the presence of the alloying elements.

The error plots for wear rate of all the alloy steels are shown in Figs 4(a-d). The wear tests were conducted thrice and the mean value was considered for analysis. The standard deviation and standard error have been found out and used for plotting the deviation of errors for the alloy steels. It is observed from the plot that the maximum standard error ($1.5x10^{-4}$) is noticed for Fe-1%C alloy steel and the minimum ($1.15x10^{-6}$) is observed for Fe-1%C-1%Ti-1%W. Similarly, the error plots are made for the coefficient of friction of all the alloy steels and shown in Figs 5(a-d). It is noticed from the calculation that the maximum standard error (0.0038) and the minimum standard error (0.002) are observed for the alloy steels containing alloying elements such as Ti, W and Ti+W. However, there is no much variation in the maximum and minimum values for standard error for the alloy steels considered for the present work.

3.4 Microstructure and Wear Pattern of P/M Alloy Steels

The microstructures of P/M alloy steels are shown in Figs 6(a-d). The optical surface morphology of the plain carbon steel is shown in Fig. 6(a). The basic microstructure observed in the steel is ferritic-pearlitic. Due to secondary heating, subsequent chemical reaction and upsetting, the lath ferrite and iron carbide have been formed and distributed in the microstructure. The iron carbides are embedded in the ferrite grains. Pearlites are observed at some places. Tiny pores are randomly distributed in the image. Due to hot upsetting and the enhancement of density of the P/M alloy steel, the pores that appeared are scarce in

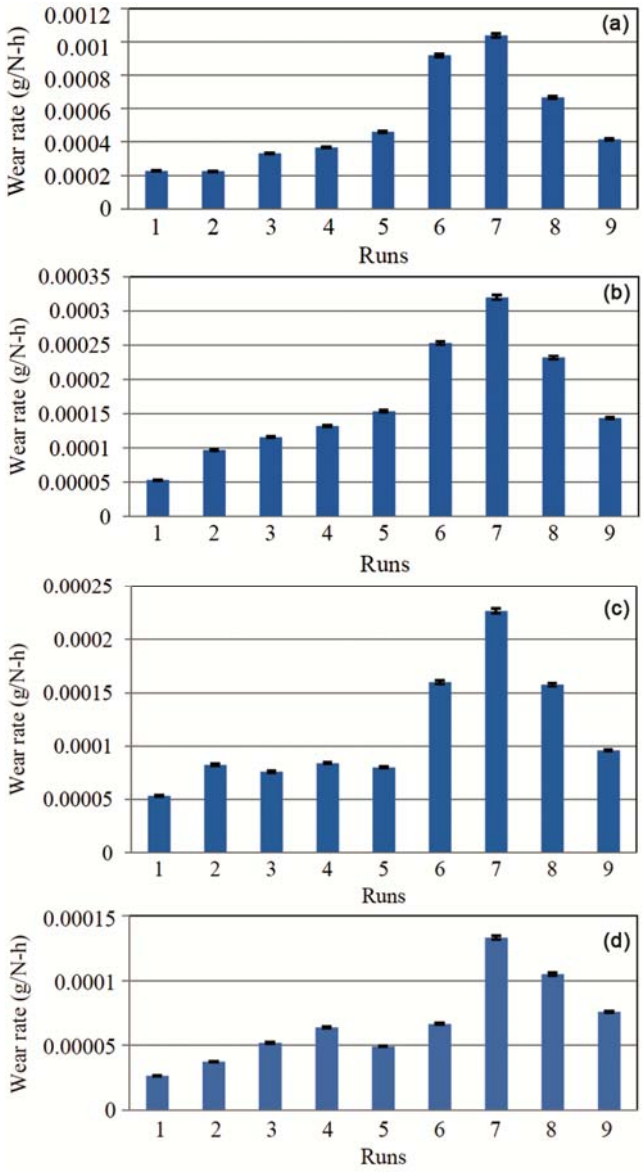

Fig. 4 — Error plots for wear rate P/M alloy steels (a) Fe-1%C, (b) Fe-1%C-1%Ti, (c) Fe-15C-1%W and (d) Fe-1%C-1%Ti-1%W.

the surface morphology of the alloy steel. Figure 6(b) shows the microstructure of Ti alloyed plain carbon steel. Elongated ferrite grains and Ti carbides embedded in the ferrite grains are observed in the microstructure. Pearlites are also seen in the microstructure. Micropores are also observed. The Ti carbides play a significant role in reducing the wear loss in the wear test. Moreover, the hardness and density enhancement improve the wear resistance of the alloy steel. However, the frictional force exerted in between the contact surfaces found to be higher. The micrograph of W added plain carbon steel is

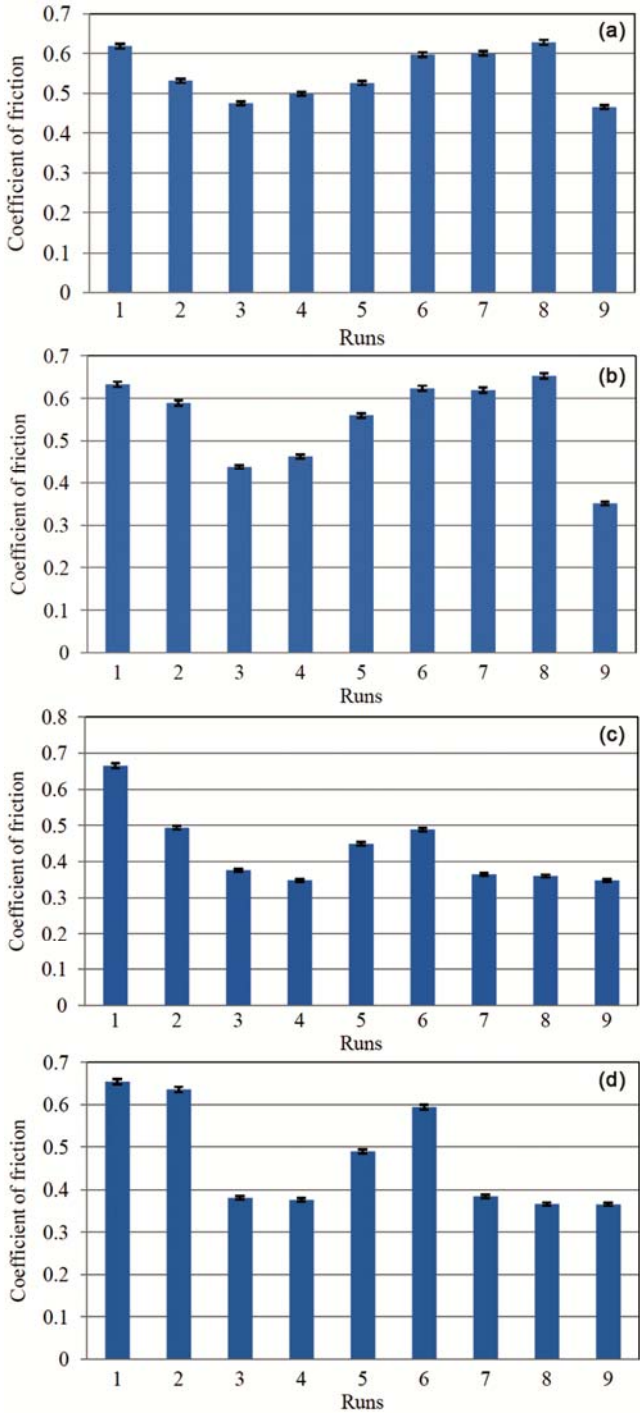

Fig. 5 — Error plots for coefficient of friction of P/M alloy steels (a) Fe-1%C, (b) Fe-1%C-1%Ti, (c) Fe-15C-1%W and (d) Fe-1%C-1%Ti-1%W.

illustrated in Fig. 6(c). Similar to the microstructure of Ti added alloy steel, elongated ferrite grains along with embedded tungsten carbides have appeared in the micrograph. Tiny pores and pearlites are also observed in the surface morphology. Formation of

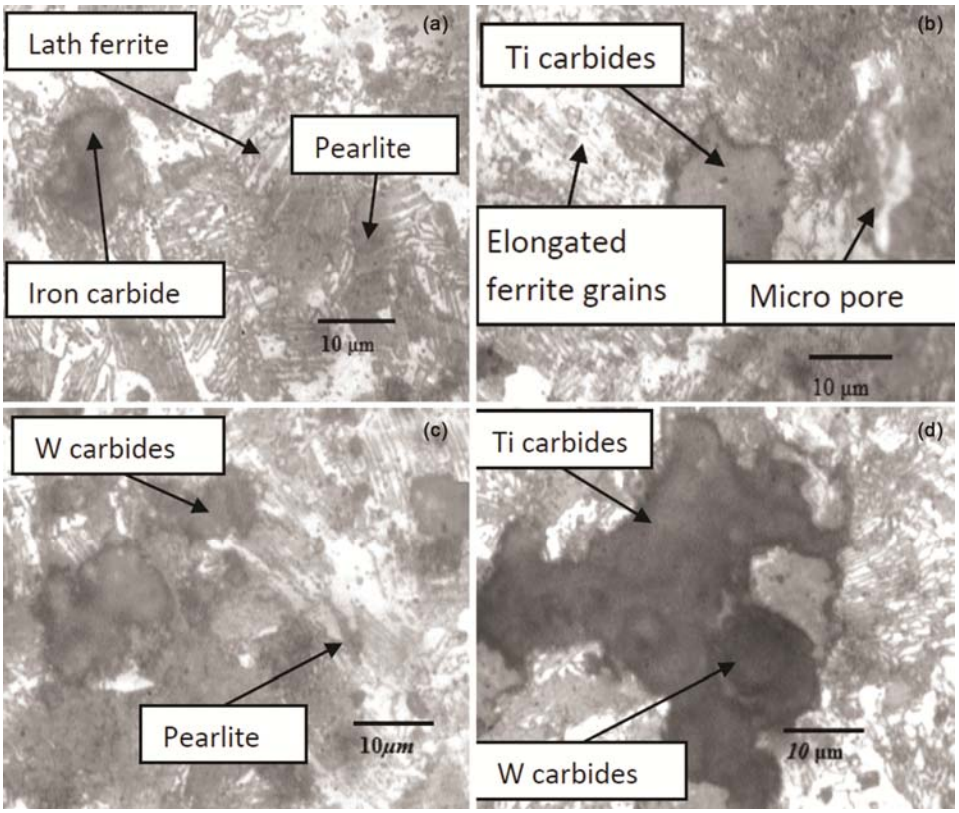

Fig. 6 — Microstructure of the P/M alloy steels (a) Fe-1%C, (b) Fe-1%C-1%Ti, (c) Fe-1%C- 1%W and (d) Fe-1%C-1%Ti-1%W.

tungsten carbides in the microstructure is found to reduce the mass loss of the alloy steel during the wear test. On the other hand, the coefficient of friction during the test is found to be higher due to the hard phases in the microstructure.

Figure 6(d) shows the microstructure of Fe-1%C-1%Ti-1%W alloy steel. The wear resistance of the alloy steel has been highly enhanced by the carbides of three elements such as Fe, Ti and W. The carbide phases are mainly occupied in the micro-image. These hard phases are found to reduce significantly the wear rate of the alloy steel. The coefficient of friction of the alloy steel during the test is observed to be the highest due to the combined effect of three types of carbides over the counter-face material.

The maximum worn out surface morphology of the alloy steels are shown in Figs 7(a-d). The wear pattern for the plain carbon steel is shown in Fig. 7(a). It is seen from the wear pattern that the maximum wear loss has occurred in the soft ferritic region rather than other areas. The image evidently shows that the mass loss has occurred to the maximum level due to non-plain and wide track appearance. Figure 7(b) illustrates the wear pattern of the Fe-1%C-1%Ti P/M alloy steel. The wear track in the image ensures the resistance of alloy steel against the wear. The non-uniform wear pattern appeared in the images is due to the presence of carbides of alloying element. The wear direction inside the track shows the direction at which the material has been ploughed during the wear test. It is evident from the wear pattern that the alloy steel has appreciable wear resistance due to the addition of the alloying element Ti and also ensures the non-uniform wear over the contact surface. The wear surface morphology of W added plain carbon steel is illustrated in Fig. 7(c). The image clearly shows that the alloy steel is subjected to non-uniform wear during the wear test. The maximum wear has taken place at the soft ferritic and pearlitic regions. The presence of tungsten carbide over the contact surface obstructs further wear on the frictional surface. The wear has taken place randomly, where the surface has soft microphases. Plastically deformed ferrite grains are also seen in the microstructure, which will further retard the material removal from the surface. The wear pattern of Fe-1%C-1%Ti-1%W P/M alloy steel is shown in Fig. 7(d). Bigger size carbide phases are observed in the image. The alloy steel is subjected to the least wear loss among the alloy steels stream. The carbides of Fe, Ti and W are

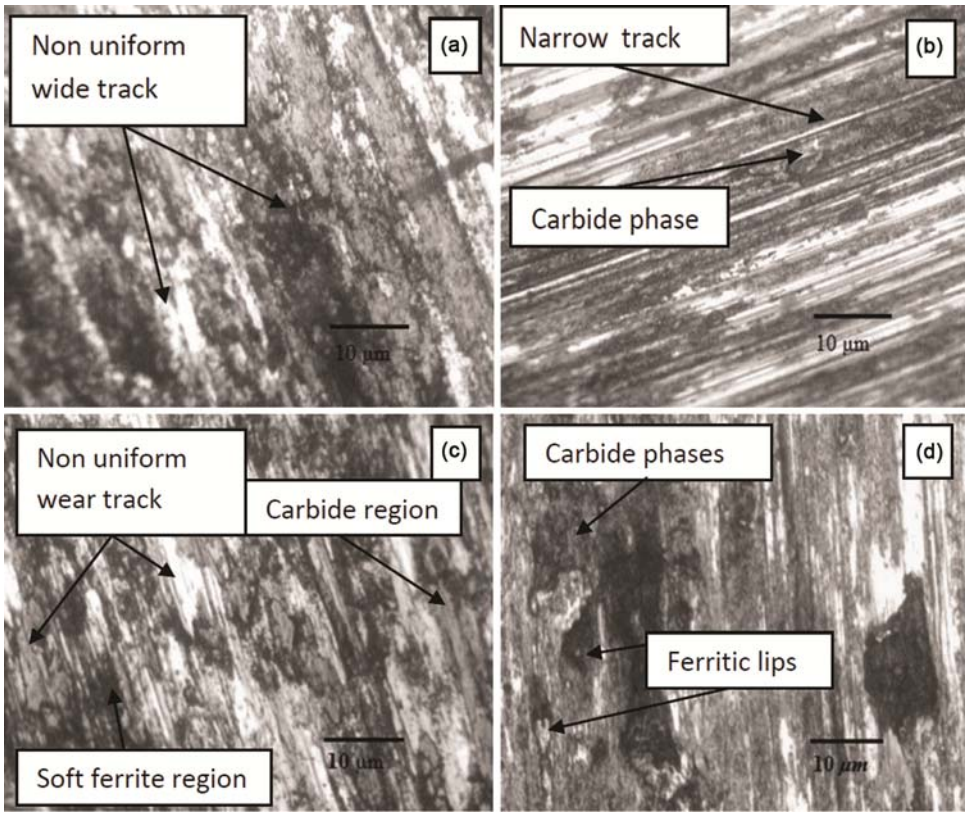

Fig. 7 — Optical wear images of the maximum worn-out surface of the P/M alloy steels (a) Fe-1%C, (b) Fe-1%C-1%Ti, (c) Fe-1%C-1%W and (d) Fe-1%C-1%Ti-1%W.

combined together and make the alloy steel harder, which invariably enhances the wear resistance of the alloy steel. Plastically deformed ferritic lips are seen at some places, which may further enhance wear resistance of the alloy steel. As the alloy steel containing the alloying elements which could form the carbides in the material, the alloy is observed to have least wear rate among the alloy steels undertaken for the research.

3.5 SEM and XRD Analyses of Wear Worn out Surfaces of P/M Alloy Steels

SEM images of wear worn out surfaces of test specimens are shown in Figs 8(a-d). It shows the SEM image of the plain carbon steel. The plain image in the figure shows the uniform wear over the entire region of the contact surface. The oxide of a chemical element is seen as white patches in the image. Iron carbides are seen as black patches. Micropores are observed randomly in the image as black tiny spot. The ridges of ferrite grains are also observed in the image. Figure 8(b) depicts the SEM image of Ti added alloy steel. It is clearly understood from the image that the specimen is subjected to non-uniform wear in the test. The wear loss has occurred in the soft ferrite region of the contact surface and the minimum wear has occurred at the carbide formed regions, which makes the wear pattern non-uniform for the alloy steel. The carbides of alloying elements are seen as black patches in some places, which reduce the material loss during the wear. Plastically deformed ferritic tongues are observed in some regions, which prevent further wear loss of the alloy steel. The oxide of material is also visible as small white patches in the image. The hardness and wear resistance of the alloy steel are enhanced by the formation of hard phases due to the alloying elements present in the alloy. The formation of carbides due to alloying element attributes for improving. The enhanced hardness due to TiC increases the abrasive action between the mating parts, which has led to increasing the frictional coefficient. SEM image of W added alloy steel is shown in Fig. 8(c). It is seen from the track that the hard particle is pulled out during rubbing action of work material with the counter body. In this alloy steel, the maximum wear has taken place over the soft ferrite region. Carbides of the alloying element embedded into the ferrite grains are also observed in the image. The formation of WC reduces the wear

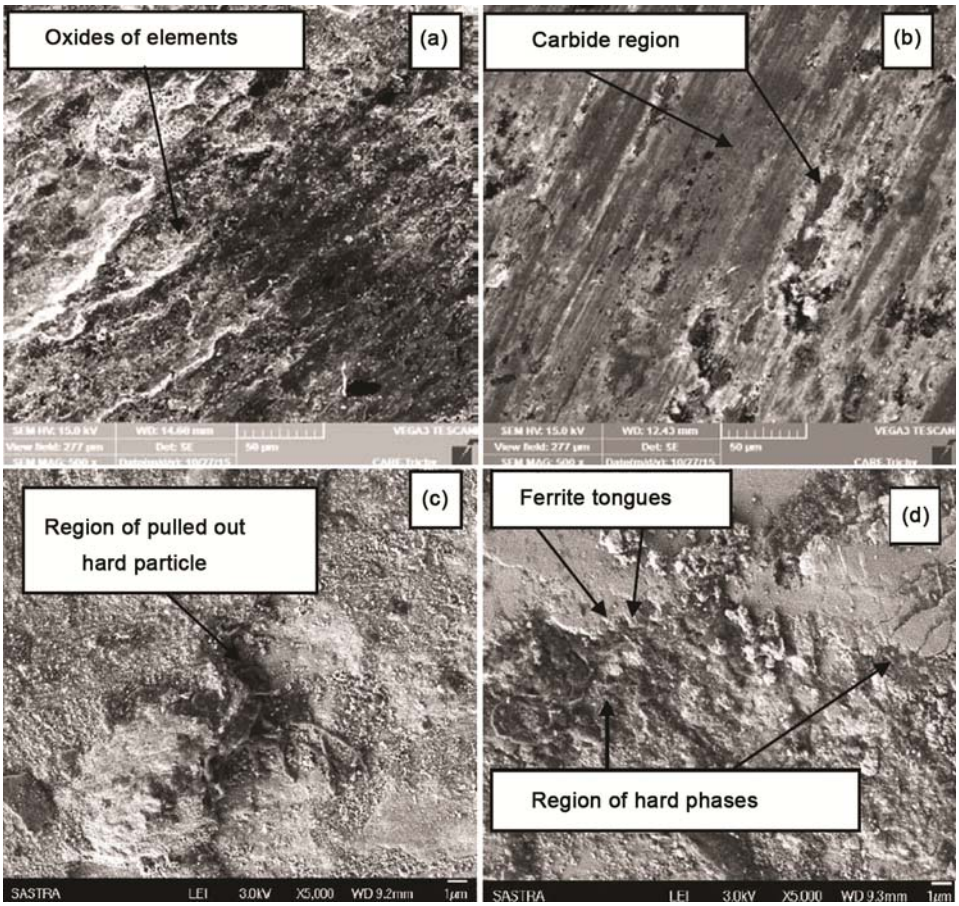

Fig. 8 — SEM images of the maximum worn out surface of the P/M alloy steels (a) Fe-1%C, (b) Fe-1%C-1%Ti, (c) Fe-1%C-1%W and (d) Fe-1%C-1%Ti-1%W.

rate and on the other hand, increases the frictional force exerted between the contact surfaces. Tiny pores are also visible in the image. Figure 8(d) shows the SEM image of Ti and W added alloy steel. It is observed through the image that the alloy steel has undergone minimal wear during the wear test. The three hard phases namely iron carbide, tungsten carbide and titanium carbide have combined and contributed to the increase in the wear resistance of the alloy steel. Carbides in the globular form are observed at some places. The plastically deformed ferrite tongues are also seen in the image.

The wear debris collected from the alloy steels during the wear tests were subjected to XRD analyses. Figures 9(a-d) show the XRD analyses of wear debris of the P/M alloy steels. The XRD analysis of the wear debris of plain carbon steel is illustrated in Fig. 9(a). The main composition of alloy steel such as iron and carbon is present in the metal powder removed from the surface of the alloy steel during wear. Moreover, the iron carbide (which is the element formed due to the chemical reaction of iron with the graphite during sintering and subsequent secondary operation) is also present in the wear debris of the plain carbon steel. The plain carbon steel is subjected to moderate wear due to the presence of iron carbide[4]. The XRD analysis of Ti added plain carbon steel is shown in Fig. 9(b). In most of the places, the titanium carbide is present along with the iron carbide. It is clearly observed from the analysis that most of the carbon present in the material is reacted with either titanium or iron and formed the concerned carbides. There is no carbon element present in the wear debris found in the analysis. It is observed from the XRD analysis that the elements such as TI_2C and Fe_2C in the alloy steel are found to enhance the wear resistance. Figure 9(c) illustrates the XRD analysis of wear debris of Fe-1%C-1%W P/M alloy steel. Similar to the Ti added alloy steel, the carbon alone is not present in the wear debris. XRD image shows that the entire graphite mixed in the composition has reacted with the iron and tungsten. The combination of carbon with iron

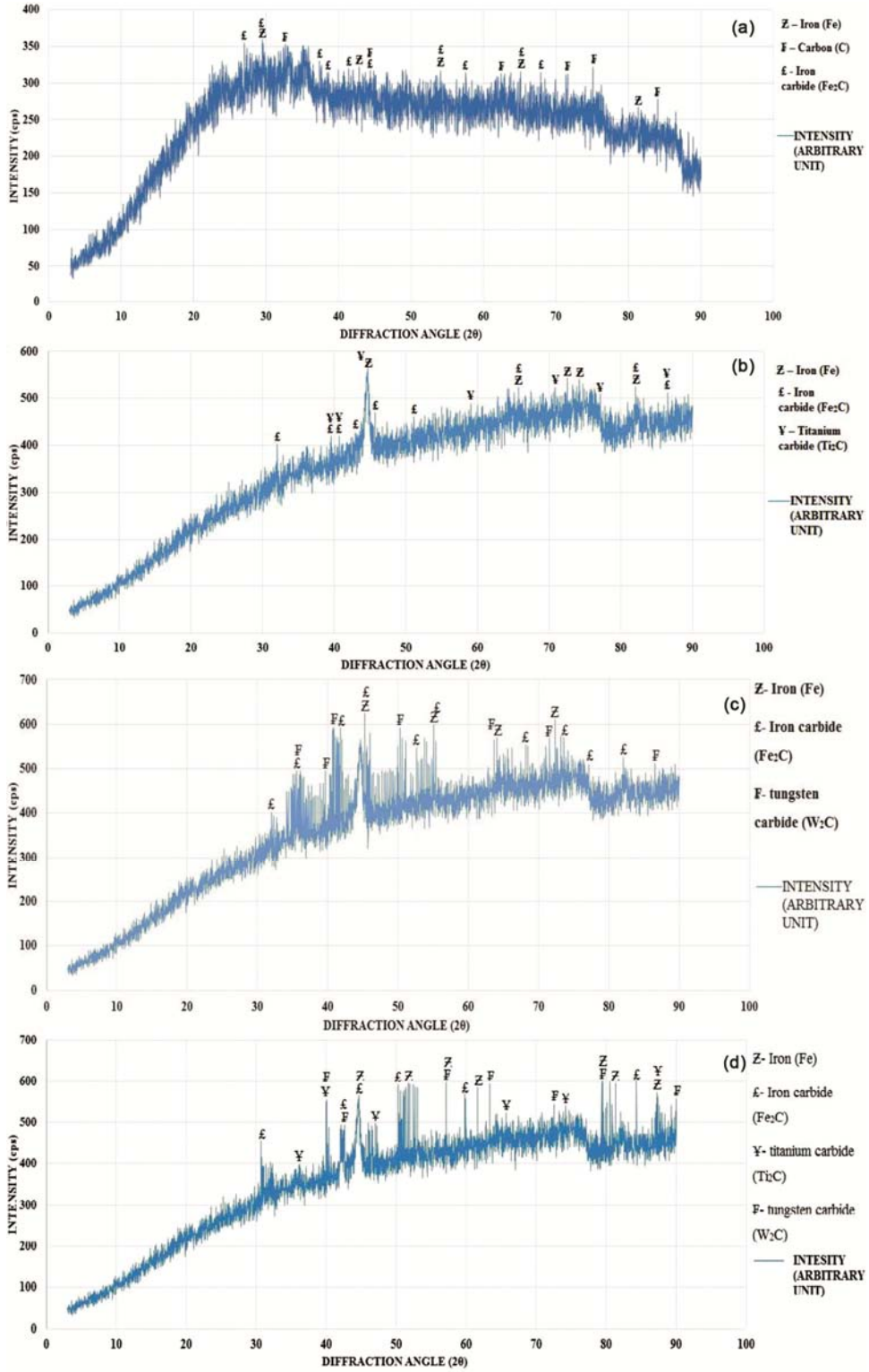

Fig. 9 — XRD peak analyses of the P/M alloy steels (a) Fe-1%C, (b) Fe-1%C-1%Ti, (c) Fe- 1%C-1%W and (d) Fe-1%C-1%Ti-1%W.

and tungsten forms Fe_2C and W_2C respectively, which are responsible for the enhanced wear resistance in the alloy. The carbides of iron and tungsten found to enhance the hardness and wear resistive property of the alloy steel. Figure 9(d) shows the XRD analysis image of Ti and W added to the P/M plain carbon steel. As expected from the chemical reaction during the sintering process that the carbides of Fe, Ti and W were formed in the alloy steel. The elements of carbides along with the base material (Fe) have been removed during the wear test as wear debris. The formation of carbides of the alloying elements contributes to the enhanced hardness as well as higher wear resistance property of the material. It is found from the wear tests of the alloy steels that the alloy steel containing Ti and W has been subjected to minimal wear loss compared to the other alloy steels selected for the research.

3.6 Application of ANN on Wear Properties of the P/M Low Alloy Steels

Mathematical correlations generated by the DE software to find the wear loss and coefficient of friction in terms of the speed and load for all the alloy systems considered for the present research work are provided in Table 3. The ANN regression plots of mass loss behavior and coefficient of friction for the P/M Fe-C-W-Ti alloy steel are shown in Figs 10(a & b). The plots are obtained by feeding the test results into the neural network toolbox. In all the cases, the trained network regression values are found to be greater than 99%. The greater values of regression confirm that the ANN model will predict the response parameters with a high accuracy level. The high level accuracy of wear property parameters could be obtained at any intermediate level of load-speed combinations from the ANN modeling due to a high level of target fitness (more than 99%). All the training, validation and test regression have been observed to be in close confirmation which indicates a good interaction between the test values and values generated from the ANN modeling. ANN is applied for other alloy steels.

The predicted values from the ANN modeling and the mathematical correlation along with the experimental results are illustrated in Figs (11 & 12) for the mass loss and coefficient of frictional values respectively for the sequential experimental runs. The error values observed by comparing the experimental values and predicted values of ANN modeling and mathematical correlations are analyzed and found to be lower. It could be concluded that the ANN modeling as well as the mathematical correlations shall be used to analyse the wear characteristics of the P/M alloy steels and these predicted values have good agreement with the experimental values.

Table 3 — Mathematical correlations for the mass loss and coefficient of friction for the P/M alloy steels.

Alloy compositions	Mass loss (Z_{ML}) Coefficient of friction ($Z\mu$)	Mathematical correlations
Fe-1%C	Z_{ML}	$(-4.76539\times10^{-3})+(1.55835\times10^{-5}X)+(1.57529\times10^{-4}Y)-(1.32808\times10^{-7}XY)-(4.157693\times10^{-9}\times X^2)+(1.02108\times10^{-6}Y^2)$
	$Z\mu$	$(0.65793)-(6.43088\times10^{-5}X)-(3.13871\times10^{-3}Y)-(7.74573\times10^{-7}XY)+(7.2853\times10^{-8}\times X^2)+(1.57865\times10^{-6}Y^2)$
Fe-1%C-1%Ti	Z_{ML}	$-(1.83012\times10^{-3})+(3.30194\times10^{-6}X)+(9.95656\times10^{-5}Y)-(4.453\times10^{-8}XY)-(1.85802\times10^{-10}X^2)-(2.0927\times10^{-7}Y^2)$
	$Z\mu$	$(0.53559)+(5.39802\times10^{-5}X)+(7.66825\times10^{-3}Y)-(3.35787\times10^{-6}XY)+(1.85296\times10^{-8}X^2)-(1.73736\times10^{-4}Y^2)$
Fe-1%C-1%W	Z_{ML}	$-(4.95249\times10^{-4})+(3.83729\times10^{-7}X)+(5.91086\times10^{-5}Y)-(2.73063\times10^{-8}XY)+(9.984896\times10^{-10}X^2)-(1.07053\times10^{-7}Y^2)$
	$Z\mu$	$(0.90123)-(2.33889\times10^{-4}X)-(1.5037Y)+(8.40934\times10^{-6}XY)-(1.27544\times10^{-7}X^2)+(6.36236\times10^{-5}Y^2)$
Fe-1%C-1%Ti-1%W	Z_{ML}	$-(6.14208\times10^{-5})-(5.37792\times10^{-7}X)+(1.68082\times10^{-5}Y)-(9.37295\times10^{-9}XY)+(1.09720\times10^{-9}X^2)+(3.31371\times10^{-7}Y^2)$
	$Z\mu$	$(0.97090)-(2.40346\times10^{-4}X)-(0.015583Y)+(8.31067\times10^{-6}XY)-(1.40944\times10^{-7}X^2)+(5.89303\times10^{-5}Y^2)$
Input parameters	X	Speed (rpm)
	Y	Load (N)

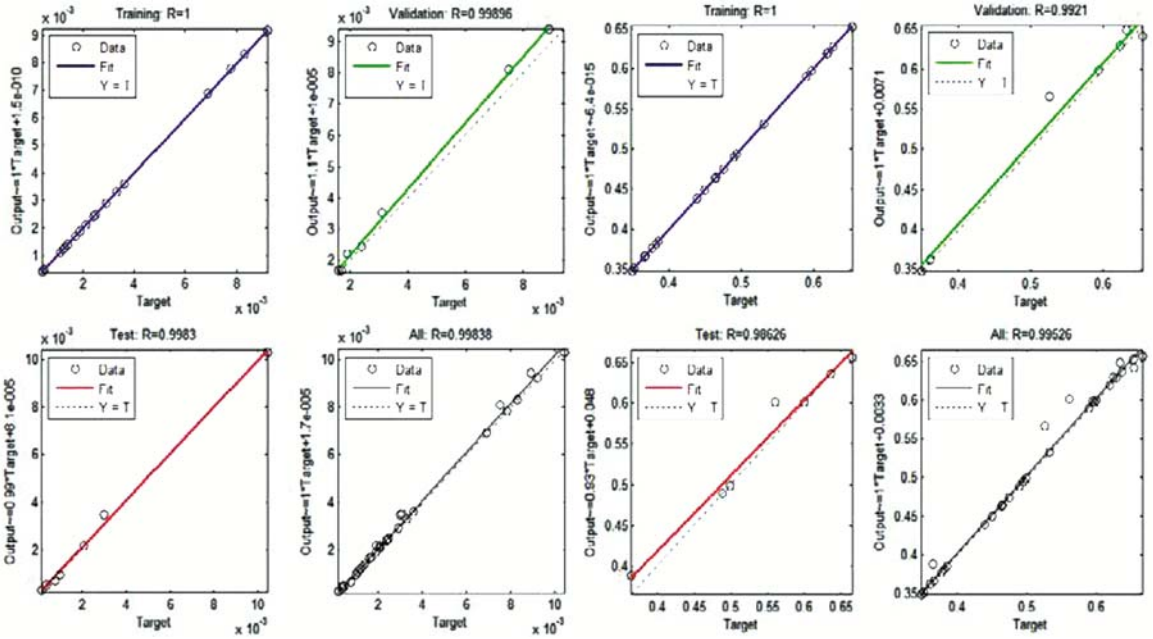

Fig. 10 — Regression plots of (a) Wear behaviour and (b) Coefficient of friction of Fe-C-W-Ti P/M alloy steel.

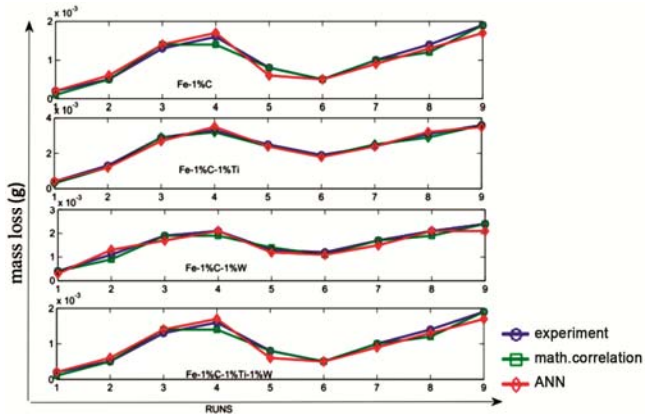

Fig. 11 — Comparison plots of mass loss values for the experimental runs.

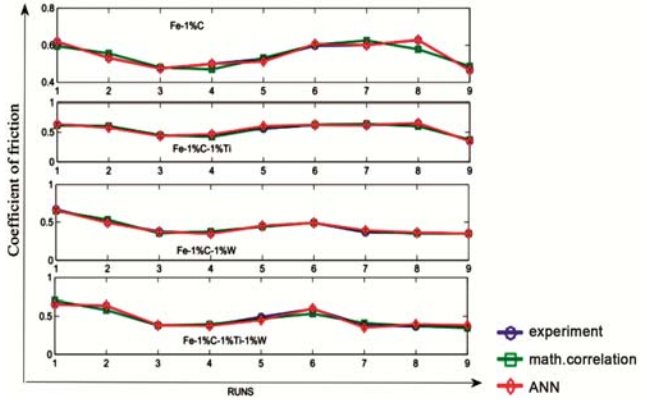

Fig. 12 — Comparison plots of coefficient of frictional values for the experimental runs.

4 Conclusions

Based on the results the following conclusions could be listed:

(i) The P/M plain carbon steel (Fe-1%C) exhibits higher mass loss and lower friction coefficient.

(ii) Addition of Ti and W to the plain carbon steel significantly enhances the wear resistance and hardness of the alloy steel due to the formation of carbides of the alloying elements.

(iii) Fe-1%C-1%W%-1%Ti shows the greatest wear resistance among the stream of P/M alloy steels selected for the experiment due to the combined effects of Ti and W.

(iv) The friction coefficient of Ti and W alloyed P/M steel is observed to be higher than that of plain carbon steel due to the formation of hard phases in the microstructure.

(v) Delamination wear mechanism is found to be common wear in all the alloy steels.

(vi) SEM and wear pattern images are clearly evident for the reduced wear loss in the case of Ti and W added alloy steels

(vii) The generalized mathematical correlations and ANN modeling for the alloy steels are generated to evaluate the mass loss and coefficient of friction and also validated with the experimental results.

(viii) The predicted results obtained from the ANN structures and mathematical equations are found well suited with the experimental results and the error between these values is also found to be low.

(ix) The interaction between the wear system and the ANN is found to be well coordinated and the ANN could be used to predict the wear properties of P/M components.

(x) The plain carbon steel is containing basic Ferritic-Pearlitic microstructure and the iron carbides are embedded in the ferritic grains.

Acknowledgements

The authors express their sincere thanks to Prof. R. Sethuraman, Vice Chancellor, SASTRA University for granting permission to publish their research work. We thank M/S Shanmugha precision forgings, a unit of SASTRA University for their support in this research work. The authors are highly thankful to M/s Hoganas India Ltd., Pune and M/s Ausbury Graphite Mills, USA, for their kind gesture in providing iron and graphite powders for the present work.

References

1 Dhanasekaran S & Gnanamoorthy R, *Mater Des*, 28 (2007) 1135.
2 Tekeli S, Gural A & Ozyurek D, *Mater Des*, 28 (2007) 1685.
3 Ozkangulsoy H, Kemalbilici M, Yahya Bozkurt & Serar Salman, *Mater Des*, 28 (2007) 2255.
4 Kandavel T K, Chandramouli R, Manoj M & Deepak Kumar Gupta, *Mater Des*, 50 (2013) 728.
5 Dhanasekaran S & Gnanamoorthy S, *Wear,* 262 (2007) 617.
6 Sudhakar K V, Sampathkumaran P & Dwarakadasa E S, *Wear*, 242 (2000) 207.
7 Song W, Zheng Ma, Zhenhua L, Jian S KeYang & Weiqiang L, *Mater Sci Eng C,* 57 (2015) 123-132.
8 Qiu J, Liua Y, Meng F, Baker I & Munroe P R, *Intermetallics*, 53 (2014) 10.
9 Wang J & Danninger H, *Wear,* 222 (1998) 49.
10 Tekeli S & Gural A, *Mater Des*, 28 (2007) 1923.
11 Aton N, Delgado J L, Velasco F & Torralba J M, *J Mater Process Technol*, 143-144 (2003) 475.
12 Vijay D & Kandavel T K, *J Adv Intelligence Paradigms,* 7 (2015) 209.
13 Lorellaceschini, G P, Giulianosambogna, D F, Giorgio S & Grazianoubertalli, *Tribology Int*, 39 (2006) 748.
14 Kandavel T K, Chandramouli R & Shanmugasundram D, *Mater Des*, 30 (2009) 1768.
15 Thanga K R S, Balaji A N, Udhaya S P & Vettivel S C, *Int J Innov Res Sci, Eng Technol,* 3 (2014) 1431.
16 Thanakrit C, Tachai L & Sombun C, *J Met, Mater Min,* 18 (2008) 17.
17 Tachai L & Patchara P, *Mater Transac*, 53 (2013) 518.
18 Róbert B, Jana B & Marco A G, *Strojarstvo*, 55 (2013) 197.
19 Vettivel S C, Selvakumar N & Leema N, *Mater Des*, 45 (2013) 323.